

High-latitude dayside energetic precipitation and IMF B_Z rotations

N. Østgaard,¹ D. L. Detrick,² T. J. Rosenberg,² R. R. Vondrak,³ H. U. Frey,¹ S. B. Mende,¹ S. E. Håland,⁴ and J. Stadsnes⁵

Received 25 February 2002; revised 8 May 2002; accepted 7 June 2002; published 21 March 2003.

[1] X-ray images from space and optical and riometer data from the ground are used to examine two discrete high-latitude dayside arcs. The dayside auroral oval is usually associated with soft precipitation of ≤ 1 keV electrons but the observed X-ray features and riometer data indicate more energetic precipitation as the X-rays are produced by electrons with energies > 2.5 keV and cosmic radio absorption is associated with ~ 10 keV electron precipitation. Both the X-ray images from space as well as the ground based optical and riometer data show two energetic precipitation events appearing at high latitudes and subsequently moving equatorward at ~ 0.5 km/s. The average energy of the electrons is estimated to be 4–8 keV, and the energy deposition is 6–10 mW/m². Owing to the high latitudes it is unlikely that these electrons were energized on the nightside and adiabatically drifted to the dayside. Instead, we think that the high-latitude events are controlled by the solar wind. The precipitation appears at ~ 77 – 79° magnetic latitude and coincides with a northward turning of the interplanetary field. Owing to the uncertainties in determining the exact location of open-closed boundary we interpret the events to be caused by either KH instabilities at the inner edge of the LLBL or by lobe reconnection. In the latter case the arcs are produced by electrons accelerated by parallel electric fields resulting from converging horizontal electric fields associated with convection enhancements due to lobe reconnection at the front surface of the magnetotail. These flux tubes map to the poleward edge of the cusp. The equatorward movement is attributed to erosion of field lines as the interplanetary field turns southward with associated dayside reconnection on flux tubes with footpoints at lower latitudes. *INDEX TERMS:* 2724

Magnetospheric Physics: Magnetopause, cusp, and boundary layers; 2407 Ionosphere: Auroral ionosphere (2704); 2784 Magnetospheric Physics: Solar wind/magnetosphere interactions; *KEYWORDS:* Magnetopause, cusp, boundary layers, auroral ionosphere, Solar wind/magnetosphere interactions

Citation: Østgaard, N., D. L. Detrick, T. J. Rosenberg, R. R. Vondrak, H. U. Frey, S. B. Mende, S. E. Håland, and J. Stadsnes, High-latitude dayside energetic precipitation and IMF B_Z rotations, *J. Geophys. Res.*, 108(A4), 8013, doi:10.1029/2002JA009350, 2003.

1. Introduction

[2] Solar wind plasma entering the magnetosphere via reconnection produces electron precipitation and optical signatures that can be monitored from ground [Rairden and Mende, 1989; Denig *et al.*, 1993; Øieroset *et al.*, 1996; Sandholt *et al.*, 1998a, 1998b]. When the interplanetary magnetic field (IMF) has a southward component, dayside reconnection with auroral signatures at the equatorward edge of the cusp (~ 73 – 75° magnetic latitude) will be observed [Sandholt and Newell, 1996; Sandholt *et al.*, 1998a] while lobe reconnection with auroral signatures at the poleward edge (~ 77 – 79° magnetic latitude) of the cusp will be seen

during northward IMF [Sandholt *et al.*, 1996; Øieroset *et al.*, 1997; Sandholt *et al.*, 2000]. The location of the merging region is also modulated by the B_Y component of the IMF with a prenoon (postnoon) displacement for positive (negative) B_Y in the Southern hemisphere, while the displacement will be opposite in the Northern hemisphere [Cowley *et al.*, 1991]. The B_X component of the IMF is also important during northward IMF, as $B_X > 0$ ($B_X < 0$) will favor lobe reconnection in the Southern (Northern) hemisphere due to the anti-parallel field condition [Crooker, 1986].

[3] Typical energies of cusp electron precipitation are ≤ 1 keV [Sandholt and Newell, 1996; Sandholt *et al.*, 1996]. However, high-latitude discrete arcs poleward of the cusp during northward IMF associated with lobe reconnection [Murphree *et al.*, 1990; Frey, 2003; Sandholt *et al.*, 2001, 2002] indicate that electrons can be accelerated to a few keVs in this region as well. Conjugate satellite passes through these arc structures by FAST (Frey *et al.*, submitted manuscript, 2002) and DMSP [Sandholt *et al.*, 2002] showed evidence of inverted-V events indicating parallel electric fields of 1–5 kV poleward of the cusp. Sandholt *et al.* [2001] suggested that lobe reconnection resulting in

¹Space Sciences Laboratory, University of California, Berkeley, USA.

²Institute for Physical Science and Technology University of Maryland, College Park, Maryland, USA.

³Laboratory for Extraterrestrial Physics, Goddard Space Flight Center, Greenbelt, USA.

⁴ISSI, Bern, Switzerland.

⁵University of Bergen, Bergen, Norway.

strong flow shears (converging electric fields) with associated sheet of outflowing field-aligned current can explain these observations of polar arcs.

[4] In the literature the poleward and equatorward edge of the cusp region is sometimes called the cleft (or exterior cusp) [see e.g. *Murphree et al.*, 1990; *Cowley et al.*, 1991]. *Woch and Lundin* [1992] and *Basinska et al.* [1992] have reported accelerated plasma at the equatorward (poleward) edge of the cusp during southward (northward) IMF conditions and suggested different acceleration mechanisms. Dayside events involving even higher electron energies (≥ 20 keV) are usually associated with central plasma sheet (CPS) electrons injected in the midnight region that subsequently drift to the dayside [*Matthews et al.*, 1988; *Newell and Meng*, 1992; *Østgaard et al.*, 1999b]. Recently such high electron energies (≥ 20 keV) have been reported during a hot flow anomaly (HFA) event [*Sitar et al.*, 1998; *Weatherwax et al.*, 1999; *Sibeck et al.*, 1999]. Energetic electron precipitation was observed by riometers and photometers from ground [*Weatherwax et al.*, 1999] when an abrupt rotations in the IMF forming a HFA was observed just upstream from the prenoon bow shock by Interball-1. HFA events are generally associated with sharp rotations in the IMF and are characterized by a rapid deflection of hot plasma from the Earth-Sun line [*Thomsen et al.*, 1986], which can be observed as a moving wave structure on the magnetopause and anti-sunward motion of (upward) field aligned current structures and optical features in the ionosphere [*Sibeck et al.*, 1999]. Cosmic radio noise absorption (CNA) enhancements associated with intensifications of the cusp currents system have been reported by *Clauer et al.* [1995] and *Stauning et al.* [1995]. These CNA events are due to electrons with energies above ~ 10 keV and indicate the presence of strong electric fields in the cleft region. Acceleration of electrons and precipitation have also been associated with Kelvin-Helmholtz (KH) instabilities. The instabilities are usually thought to result on the dawn and dusk flanks of the magnetosphere as the solar wind flows past, but they can also occur at shear flow boundaries on the inner edge of the low latitude boundary layer (LLBL) [*Clauer et al.*, 1997].

[5] In this study we report two high-latitude discrete arcs that were observed on May 8, 1998 (1345 UT and 1407 UT) over the South Pole station (1030 MLT) involving electrons with an average energy of 4–8 keV. The two events were observed by riometer, all-sky-cameras (ASC) and photometers at the South Pole station and by X-ray imaging camera from space. Both events were first seen as discrete arcs at high latitudes (~ 77 – 79° magnetic latitude) with subsequent movements to lower latitudes ($\sim 73^\circ$). Our observations indicate that these electrons did not originate on the nightside and drift adiabatically to the dayside, but were rather accelerated locally by processes controlled by the solar wind. Different candidate mechanisms that may produce discrete arcs at such high latitudes are discussed. The subsequent equatorward motion is attributed to the erosion of fieldlines due to the IMF rotation from northward to southward.

2. Data and Instruments

[6] The X-ray imaging data from space were obtained by the Polar Ionospheric X-ray Imaging Experiment (PIXIE)

onboard the Polar spacecraft. PIXIE is a pinhole camera providing X-ray measurements in the energy range ~ 2.5 – 22 keV. When the Polar satellite is at perigee the camera provides X-ray images with a spatial resolution of ~ 170 km. Due to the low altitude at perigee (~ 5000 km) the higher count rates allow us to fully utilize the adjustable time resolution of the PIXIE camera. We first accumulate images for 20 sec and then add 3 time frames to obtain 1 min time resolution. By doing this we get significant count rates in the 6 energy bins of X rays we use to derive electron energy spectra without decreasing the spatial resolution (the Polar satellite moves 80 km in 20 sec at perigee). Due to its large field of view (FOV), the PIXIE camera provides close to global coverage even when Polar is at these low altitudes. The X rays measured by PIXIE are produced by electrons from ~ 2.5 keV to 100 keV. A detailed description of the data processing from PIXIE is given by *Østgaard et al.* [1999a] and details on deriving four-parameter electron spectra from PIXIE measurements are given by *Østgaard et al.* [2000, 2001].

[7] The optical data from the ground were collected from the South Pole station located at 74.02°S and 18.35°E in corrected geomagnetic (CGM) coordinates. Data from two photometers and a two-wavelength all-sky-camera (ASC) were used in this study. We have used meridian slices of the ASC data to present keograms in the same format as shown by e.g., *Mende et al.* [2001]. One photometer and the ASC measure the atomic Oxygen (OI) emission line at 630.0 nm. This is not a prompt emission (lifetime 110 sec) and is consequently suppressed due to non-radiative processes at lower altitudes where the atmosphere gets denser. The OI line therefore reflects the soft electron precipitation (< 1 keV) and the average peak intensity is taken to be at ~ 200 km altitude (used for the keogram from ASC data), which may be a lower altitude estimate as discussed below. The other photometer and the ASC measure the singly ionized molecular Nitrogen (N_2^+) emission line at 427.8 nm. This is a prompt emission and proportional to the total energy flux of the precipitating electrons. All electron energies contribute in the production of these emissions and for the keogram derived from the ASC data the average peak intensity is assumed to be at ~ 110 km (corresponding to maximum energy deposition of ~ 7 keV electrons, according to *Rees* [1963]), which also is a lower altitude estimate as will be discussed. From the intensity of the 427.8 nm emissions the total electron energy flux can be estimated. As these two emission lines are sensitive to different electron energies, the ratio of the two intensities can be used to extract information about the average energy of the precipitating electrons [*Eather and Mende*, 1971; *Rees and Luckey*, 1974; *Rees and Roble*, 1986]. The two photometers with a 55° full angle FOV are used to derive energy characteristics of the electron precipitation.

[8] The cosmic radio noise absorption (CNA) at 38.2 MHz was measured by the imaging riometer [*Detrick and Rosenberg*, 1990], whereas a broadbeam riometer measured the CNA at 30 MHz at the South Pole station. The attenuation of cosmic radio noise depends exponentially on the absorption coefficient, which in turn is proportional to the electron density (n_e) and the collision frequency between electrons and neutral particles (ν). As ν falls off rapidly with height due to decreasing neutral density, the

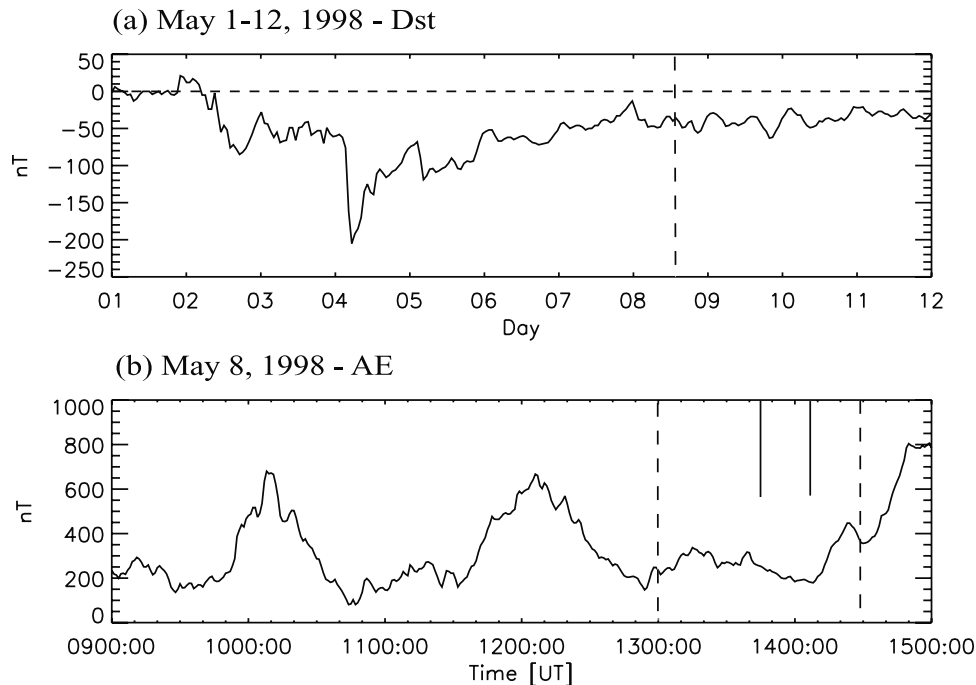


Figure 1. (a) Dst index May 1–12, 1998. (b) AE index May 8, 1998. The dashed lines indicate the time interval we focus on. The two solid lines indicate the onset of the high latitude dayside precipitation events.

CNA is usually not very significant above ~ 100 km, i.e., at the altitude of maximum energy deposition for 10 keV electrons [Rees, 1963]. This implies that most absorption occurs at altitudes below ~ 100 km where electrons in the energy range from 10 keV to 100 keV deposit their energy [Berkey *et al.*, 1974]. The FOV of the imaging riometer is a factor 5 smaller than the FOV of the ASC (radius of ~ 100 km compared to ~ 500 km for the ASC). The broadbeam riometer which is used to derive energy characteristics of the electron precipitation has an approximately 60° full angle FOV that matches the FOV of the photometers described earlier.

[9] The solar wind density and velocity and measurements of the interplanetary magnetic field (IMF), with a time resolution of 79 s and 46 s, respectively, were available from the solar wind experiment [Ogilvie *et al.*, 1995] and the magnetic field experiment [Lepping *et al.*, 1995] on board the Wind spacecraft.

3. Observations

[10] Figure 1 shows geomagnetic conditions encompassing our events from 1300 UT to 1430 UT on May 8, 1998. Dashed lines (Figure 1b) show the time interval we focus on and solid lines indicate the onsets of the two arcs (1345 UT and 1407 UT). Dst (Figure 1a) is still significant at -40 nT during this recovery phase of a magnetic storm (-205 nT) that occurred 4 days earlier. The AE index (Figure 1b) indicates that a substorm occurred between 1135 UT and 1255 UT. At 1410 UT there was another increase related to a new substorm in progress in the midnight sector, but this increase occurred too late to affect the dayside precipitation we examine in this paper. Ground based magnetometers in

the midnight sector (MM 210, not shown) as well as geosynchronous satellite data (not shown) confirm this picture of no substorm activity during the time interval we examine. As seen in Figure 2i, the H-component measured at the South Pole station does not indicate any substorm activity either. We therefore conclude that our dayside events were neither magnetic storm nor substorm related, but occur during late recovery of both a substorm and a magnetic storm.

[11] The two upper panels in Figure 2 show the keograms derived from the ASC data at the South Pole, from 1300 UT to 1430 UT (0930–1100 MLT). The red 630.0 nm emission line (Figure 2a) is due to soft (<1 keV) electrons while the blue 427.8 nm emission line (Figure b) is due to a few keV electrons. Although the FOV is similar for the two wavelengths of the ASC the different altitudes of peak intensity result in different ranges of magnetic latitudes. Figure 2c shows keograms derived from the imaging riometer. Notice that the riometer FOV is a factor 5 smaller than the ASC FOV. The 200 km FOV corresponds roughly to 2° magnetic latitude, which means that we obtain keograms from -73° to -75° . In the next five panels we show the solar wind data; Figure 2d shows the clock angle of the IMF, defined as the polar angle between the IMF as projected into the Y-Z plane and the Z-axis in GSM coordinates, Figures 2e–2h show IMF B_Z , IMF B_Y , IMF B_X and the solar wind dynamic pressure, respectively. The solar wind data are shifted 41 min to take into account the solar wind propagation time from the Wind satellite location at [211, 7.6, 30] R_E in GSM coordinates to the subsolar magnetopause (at 10 R_E). This time shift also includes 5 min to approximate the braking of the solar wind at the bow shock and the propagation from the magnetopause to the ionosphere. During the time

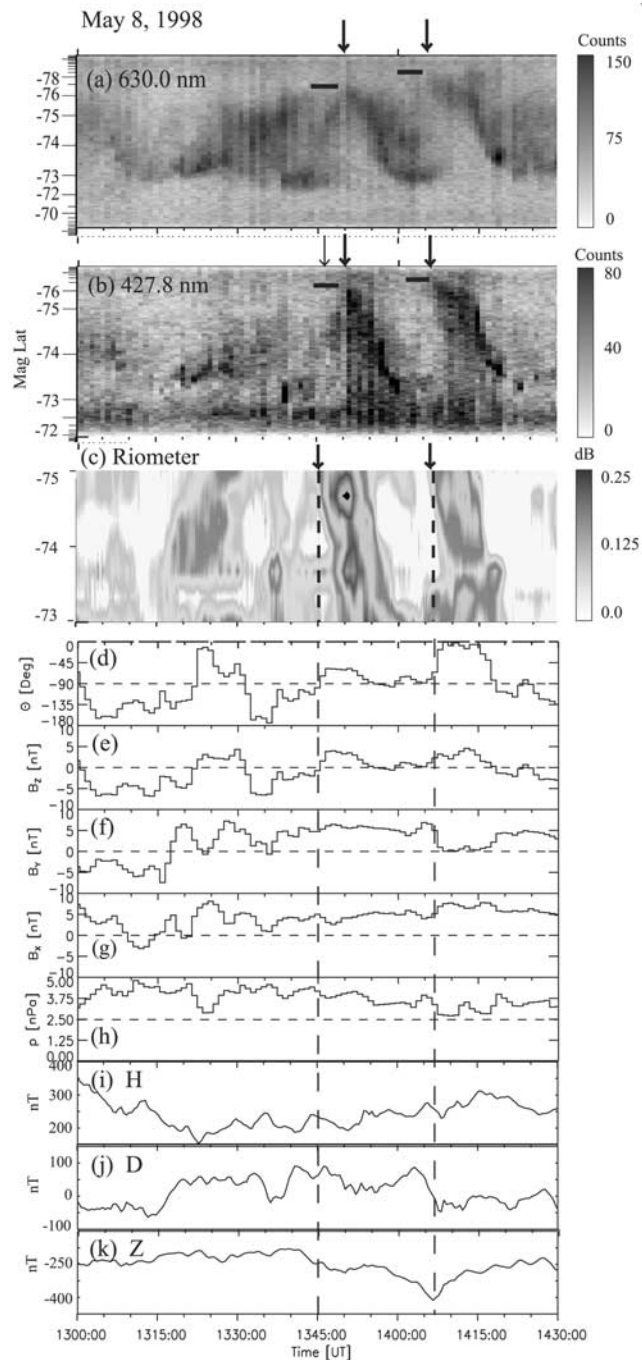


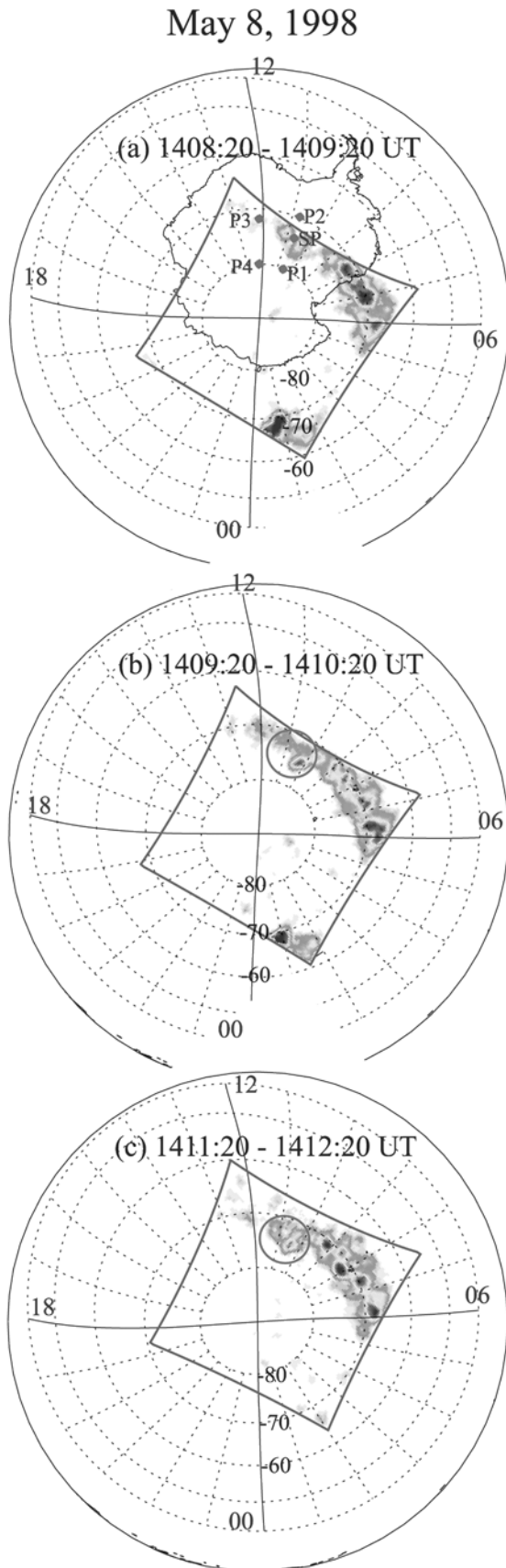
Figure 2. The three upper panels show meridian slices of the ASC and riometer data from the South Pole station, presented as keograms. (a) 630.0 nm emissions (<1 keV electrons). (b) 427.8 nm emissions (~ 10 keV electrons). (c) 38.2 MHz CNA (~ 10 –100 keV electrons). Arrows indicate the onset times of the high latitude precipitation. Red (black) horizontal lines indicate the latitude of the onsets. The five next panels show the solar wind data. (d) θ is the IMF clock angle from 0° (northward) to 180° (southward). (e) IMF B_z (f) IMF B_y (g) IMF B_x (h) Solar wind dynamic pressure. Dashed line indicates average solar wind pressure. The three bottom panels (i–k) show the magnetic data from the South Pole station. See color version of this figure at back of this issue.

interval shown in Figure 2 the solar wind velocity stays constant at 600 km/s (which is above the average speed; 400 km/s, data not shown) and the dynamic pressure varies slightly (3–5 nPa, see Figure 2h) which is also above the average value (2.5 nPa). The last 3 panels (Figures 2i–2k) show the magnetic data from the South Pole station. Both the ASC keograms and the riometer keogram show two distinct features of arc structures at high latitudes with subsequent equatorward movements. The thick arrows indicate the onset times of the two events. For the first event (1345 UT and ~ 1015 MLT) the riometer arc seems to precede the ASC arcs (1350 UT) by 5 min, but looking at the 427.8 emission an intensity increase is seen between -75° and -74° simultaneously with the riometer peak at $\sim -74.8^\circ$ CGM latitude. We therefore attribute the apparent time lag to the riometers limited FOV. The second event, 20 min later, was observed simultaneously in all three panels (1407 UT and ~ 1035 MLT). The red line (630.0 nm) indicates that the first event starts at $\sim 77^\circ$ and the second one at $\sim 79^\circ$ and they both move to $\sim 73^\circ$ in about 10 min, which gives an equatorward velocity of ~ 0.5 km/s. It should be noticed that these latitudes are lower estimates as we have used a low altitude estimate of the peak intensity for both 630.0 nm and 427.8 nm (200 km and 110 km, respectively). During the events IMF B_y and B_x are positive (Figures 2f and 2g) and both events begin with distinct northward clock angle (θ) turnings. Subsequent southward turning coincides with the equatorward movement of the arcs.

[12] During one of these events the Polar satellite made a perigee pass and the PIXIE camera provided images of the dayside aurora from 1408–1413 UT, which enables us to view the second event from space.

[13] In Figure 3 we show three of the X-ray images during this 5 min time interval. The large red circle shows the FOV of the ASC. In the first image (1408:20–1409:20 UT) X rays are seen between -73° and -77° CGM latitude which is consistent with ASC keograms and riometer data at that time (Figure 2). In the last image (1411:20–1412:20 UT) the high-latitude X-ray feature has moved equatorward a degree or so, but is still separated from the morning side precipitation which is seen in all the images at lower latitudes (equatorward of -73°) from 6 to 10 MLT.

[14] The photometer and broadband riometer data from the South Pole and the X-ray data from space enable us to estimate the energy characteristics of the electron precipitation using three different methods. The photometers with a 55° full angle FOV looking towards zenith at the South Pole are used for this calculation, which explains why the peaks are slightly delayed relative to the times indicated in Figure 2. In the three upper panels of Figure 4 we show the timeseries of (Figure 4a) the 630.0 nm emissions, (Figure 4b) the 427.8 nm emissions and (Figure 4c) the 30 MHz broadband riometer. The two lower panels show (Figure 4d) the average energy and (Figure 4e) the energy flux of the precipitating electrons based on the different methods. The solid line shows the result based on the 630.0 nm and 427.8 nm emission lines following the procedure described by Rees and Luckey [1974] and Rees and Roble [1986], who used Maxwellian electron distributions to model emission ratios. The intensity ratio of the two lines is used



to estimate the average energy but as the intensity of 630.0 nm emission approaches zero for electrons above 1–2 keV this method is not very accurate for average energies larger than ~ 2 keV. The dashed line is based on the absorption of 30 MHz cosmic radio noise and the 427.8 nm emission line which allow us to estimate higher average energies. This technique uses a computer code developed at the University of Maryland based on the TANGLE code [Vondrak and Baron, 1976; Vondrak and Robinson, 1985] and the formulas from Rees [1989]. This code is described in more detail by Aksnes *et al.* [2002]. Maxwellian electron distributions were used in this calculation. The average energy estimated from X rays (shown by horizontal thick line) is estimated from the 2.5–22 keV X-ray spectrum which gives us a double exponential electron spectrum from 2.5 keV to ~ 100 keV [Østgaard *et al.*, 2001]. In Figure 4d we have plotted the average energy between 1410 UT and 1414 UT in the energy range from 2.5 keV to 100 keV, which may be higher than the average estimated from the other methods as the photometers respond to the lower part of the electron spectra which is not seen by the PIXIE camera. Although the average energy derived from the three methods varies they indicate that the average energy is between 4 keV and 8 keV, if the average energies based on the 630.0 nm emission line are disregarded for reasons mentioned above. The energy flux is very similar for the solid and dashed line which is reasonable because they are both estimated from the 427.8 nm emission line. The mean energy flux between 1410 UT and 1414 UT derived from the X rays confirm an energy deposition rate of 6–10 mW/m² during the two events. The peaks of the energy flux lag the peaks of the average energy. This apparent softening of the spectra during the events is not real but rather due to the long lifetime of the 630.0 nm emission (110 s). The observed time delay is close to the 3 min modeled estimate of the delay between the initiation of precipitation and the peak of the emission reported by Roble and Rees [1977]. The reason for not using the ASC data for this calculation is that the photometers and ASC are not intercalibrated. The FOV of the photometers and riometer correspond to a 50 km radius circle at 100 km (riometer and 427.8 nm) and 100 km at 200 km (630.0 nm), which are comparable to the spatial resolution of PIXIE (170 km \times 170 km). The results are therefore averages within these areas. Although the form of the incident electron distribution used to determine the energy characteristics will affect the results slightly, the accuracy of our results are mostly determined by the calibration accuracy. For the energy characteristics derived from PIXIE, the X-ray count rates will determine the accuracy. Considering the different sources of uncertainties and limitations of the methods we are not able to determine the energy characteristics precisely but our results give

Figure 3. (opposite) 2.5–9.0 keV X-ray images on a CGM grid, 1 min time resolution from (a) 1408:20–1409:20 UT (b) 1409:20–1410:20 UT and (c) 1411:20–1412:20. The distorted red squared box indicates PIXIE FOV and the large red circle in (b) and (c) indicates the ASC FOV. The South Pole station and the AGO stations are indicated in (a). See color version of this figure at back of this issue.

May 8, 1998

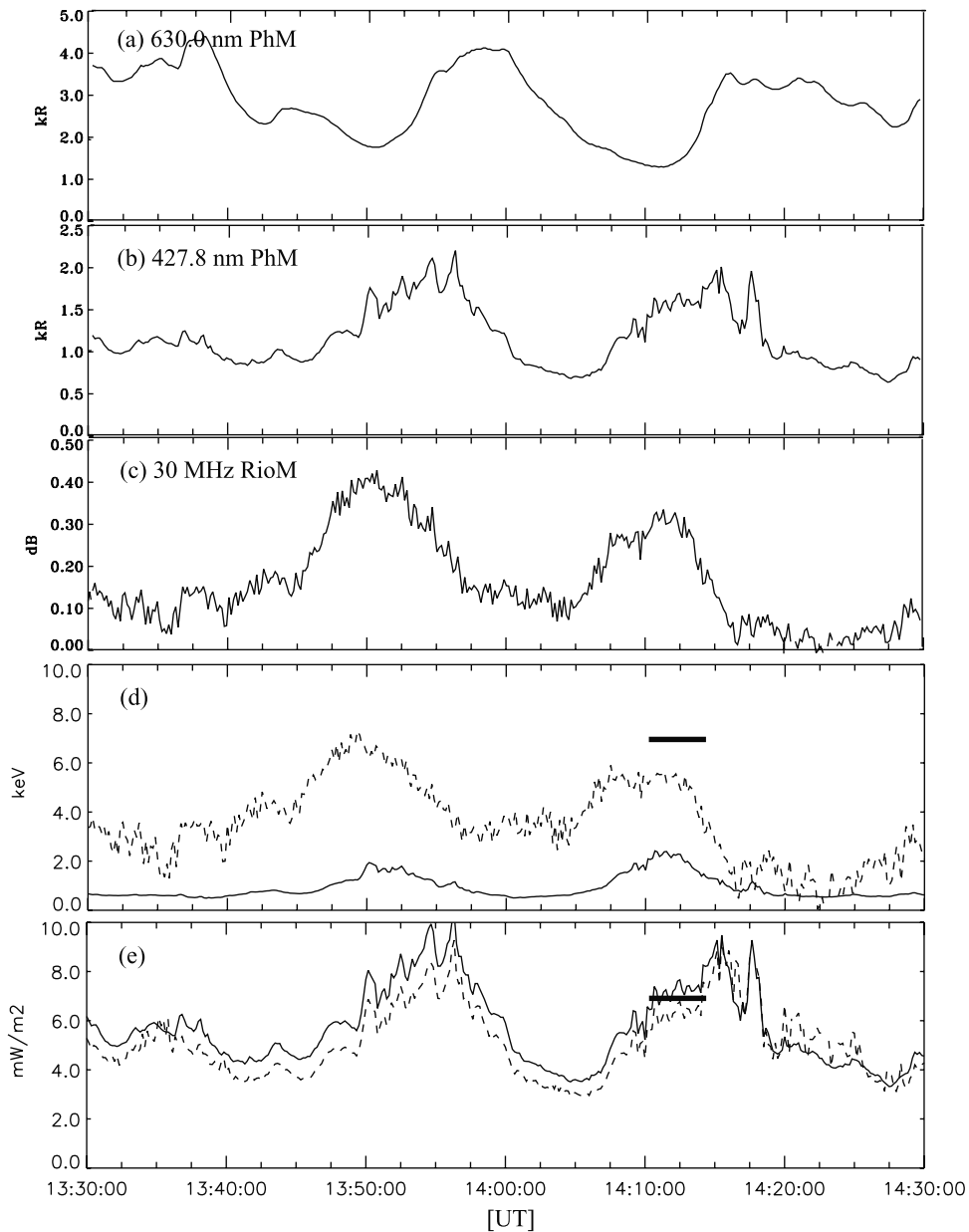


Figure 4. (a) 630.0 nm photometer (b) 427.8 nm photometer. (c) 30 MHz broadbeam riometer. (d–e) Energy characteristics of the precipitating electrons estimated from photometer, broadbeam riometer and X-ray data. (d) The average electron energy. (e) The electron energy flux. Solid line: Based on 630.0 nm and 427.8 nm emission lines. Dashed line: Based on absorption of 30 MHz cosmic radio noise and photometer 427.8 nm emissions. Thick solid line: Average values for 1410–1414 UT based on the X-ray measurements.

strong indication of average energies of 4–8 keV and energy flux of 6–10 mW/m².

4. Discussion

[15] Is this a purely dayside phenomenon controlled by the solar wind or are these electrons energized on the nightside and adiabatically drifted to the morning sector? In the latter case this will correspond to Boundary Plasma Sheet (BPS) or Central Plasma Sheet (CPS) electrons. Using

low altitude satellite measurements *Newell and Meng* [1992] identified different electron populations and found that electron distributions with BPS characteristics statistically extend to 10 MLT at 75–76° magnetic latitude. In a study by *Matthews et al.* [1988] two electron precipitation events involving energies from 20 keV to 250 keV were observed by balloon-borne X-ray detectors over the South Pole station. Due to dispersion signatures one of the events was explained as drifting electrons from a midnight injection, while the other event was interpreted as electrons being

scattered into the loss cone close to the station. In the present study we see electrons with average energies of 4–8 keV and due to the CNA features the fluxes of >10 keV electrons also have to be significant. Although the energy characteristics of the electrons are similar to BPS (or CPS) electrons we have reasons to doubt such an explanation. Using the Tsyganenko 1996 model [Tsyganenko, 1995] parametrized with realistic solar wind input parameters we found that the X-ray features over the South Pole station map to the boundary of open-closed field lines (not shown). Due to the uncertainties of mapping results we will not interpret this as more than a weak indication of a source region in the magnetosheath. Although there were no passes by low-altitude satellites through this region in the southern hemisphere, DMSP F14 passed through the same local times in the northern hemisphere 5 min prior (1340 UT) to the first event. These measurements (not shown) indicate that the cusp was located at $\sim 76^\circ$ CGM latitude, the LLBL between 75 and 76° CGM latitude and that the CPS was encountered at $\sim 74.5^\circ$ CGM latitude. We have also looked at the flux-gate magnetometer data from the Automatic Geophysical Observatory (AGO) stations and at the South Pole. Following the procedure described by Lanzerotti *et al.* [1999] the dynamic power spectra of the H and D component of the magnetic field can be used to locate the boundary between open and closed field lines. Power spectra from the AGO stations and the South Pole (not shown) indicate that the open-closed boundary lies equatorward of the South Pole station at -74° CGM latitude (personal communication, L. J. Lanzerotti, 2002). An open-closed boundary equatorward of the South Pole is consistent with the above-average solar wind pressure, which results in a compressed magnetopause [Shue *et al.*, 1997, 1998]. This brief discussion leads us to believe that the open-closed boundary in the southern hemisphere was somewhere between -74° and -76° CGM latitude. The arcs we see in the ASC keograms are formed at -77° and -79° . This means that they are either formed poleward of the cusp or that the IMF northward turning moved the open-closed boundary to such high latitudes that the arcs were formed just equatorward of the cusp.

[16] Are these arcs the same features we observe in CNA and X rays? As the riometer FOV does not extend poleward of -75° CGM latitude we cannot be certain that CNA would be seen at -77° and -79° CGM latitude where the arcs formed. However, Figure 2c shows that the CNA features originated beyond our FOV and we therefore think it is very likely that we see the CNA features as they moved above the South Pole station from high to lower latitudes (Figure 2c). The imaging riometers from the AGO stations P1 (-80.1° CGM latitude and 1140 MLT) and P4 (-80.0° CGM latitude and 1200 MLT) both with a similar FOV as the South Pole riometer (2°) did not show any signature of enhanced absorption (not shown). The first X-ray image (Figure 3a) shows X-ray features from -73° to -77° CGM latitude, while the last image (Figure 3c) shows a slight equatorward movement by a degree or so. The morning precipitation at lower latitudes (equatorward of -73°) is seen from 6 to 10 MLT and is separated from high-latitude precipitation. The spatial resolution of the PIXIE camera of 170 km explains why this separation is not so clearly seen in the X-ray images as in the ASC keograms.

[17] Our observations might have been due to some anomalously large fluxes of energetic (>10 keV) electrons in the solar wind, but neither ACE [at L1], Wind [211, 7.6, 30 R_E in GSM coordinates] or Geotail [$-1, 30, -2 R_E$ in GSE coordinates] show any signatures of such electrons (data not shown). One possible mechanism that would result in auroral features as we observe at the South Pole is the passage of a hot flow anomaly (HFA) as reported by Sibeck *et al.* [1999] and Weatherwax *et al.* [1999]. Such an anomaly should be related to very sharp discontinuities in the IMF, which are not apparent in our data. As abrupt IMF B_Y and B_Z changes might have been averaged out in the 1 min data we also checked the 3 sec resolution data from WIND. Except for small-scale variations, the high-resolution data show similar changes as the 1 min data during the two events. Magnetic measurements from Geotail and Interball-1 (both located just upstream from the bow shock, data not shown) also confirm the 1-min WIND data as well as the time shift of 41 min we have applied. Magnetic field measurements from South Pole (Figures 2i–2k) do not show the abrupt large amplitude disturbances that are expected during HFA events. The Z-component shows a step-like decrease during the two events and the D-component shows a rotation during the second event but the H-component is fairly stable during both events. Magnetic data from the Automatic Geophysical Observatory (AGO) stations (P2, P3 and P4, data not shown) do not show any abrupt large amplitude disturbances either. Instead of anti-sunward motion of the optical signatures as predicted by Sitar *et al.* [1998] and observed by Sibeck *et al.* [1999] we observe an equatorward movement of the optical features. We conclude that our data do not give very strong support for the HFA hypothesis. However, as HFAs have not been observed very often the characteristics of such events are not very well established and we should be cautious to rule out such an interpretation completely.

[18] KH instabilities are typically thought to be found on the flanks of the magnetopause, but they have also been reported to occur at the inner edge of the LLBL [Clauer *et al.*, 1997, and references therein]. On the dayside, the LLBL maps to the ionospheric convection reversal [Newell and Meng, 1992] equatorward of the cusp. If the open-closed boundary is between -74° and -76° CGM latitude as discussed earlier the arcs are formed poleward of the convection reversal location. On the other hand, if the cusp has moved significantly poleward due to the IMF northward turning, KH instability can very well be the mechanism that produces these arcs. The X-ray features we observe at lower latitudes in the morning sector (06–10 MLT) (Figure 3) may also be associated with KH instabilities.

[19] The two events can also be explained by high-latitude lobe reconnection with a subsequent erosion of field lines when the IMF turns southward. We first notice that the geometry of field lines (see the sketch in Figure 5) with the dipole tilted towards the sun (May 8), IMF B_Z and IMF B_X both positive favors lobe reconnection on the front surface of the magnetotail in the Southern magnetosphere on flux tubes with footpoints poleward of the cusp [Crooker, 1986], as indicated in Figure 5a. The positive IMF B_Y will tend to locate the merging region prenoon in the Southern hemisphere, as indicated in Figure 5b (opposed to a postnoon displacement in the Northern

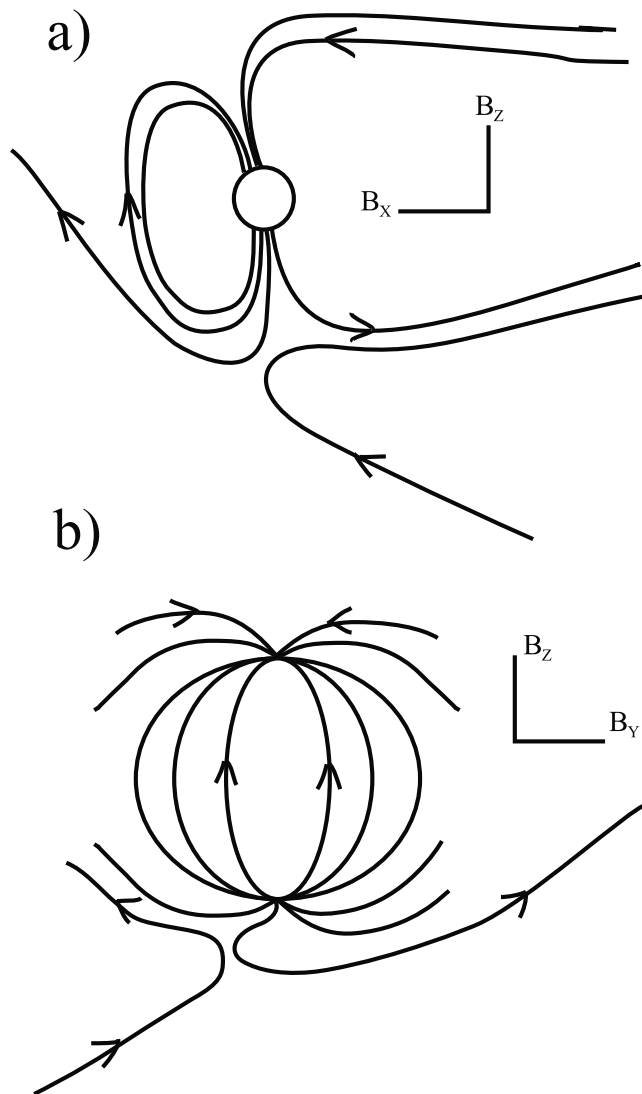


Figure 5. Sketch of the field line geometry and merging location when IMF is northward and both B_Y and B_X are positive. (a) Meridian scan of the magnetosphere. (b) The magnetosphere viewed from the Sun.

hemisphere). Auroral signatures corresponding to lobe reconnection have been reported in many studies using scanning photometers at 630.0 nm emission and 557.7 nm emission [see, e.g., Sandholt *et al.*, 1996, 2000; Øieroset *et al.*, 1997]. The auroral signatures which have been termed type 1 aurora [Sandholt *et al.*, 1998b] are usually most intense in the 630.0 nm emission line, which indicates soft electron precipitation (<1 keV), but often show up as significant 557.7 nm emissions, indicating higher electron energies as well [Sandholt *et al.*, 2001]. Murphree *et al.* [1990] reported several cases of high-latitude discrete auroral arcs observed in UV emissions by the VIKING satellite. They related these structures to lobe reconnection at the front surface of the magnetotail although the discrete arc structures indicated precipitation by a few keV electrons. Frey [2003] examined 2 months of IMAGE FUV data and found 13 events covering 73 hours of observations

where UV arcs were seen poleward of the cusp during northward IMF. In situ measurement by the FAST satellite passing through the arcs provided clear evidence of inverted-V events, indicating parallel electric fields of 1–5 kV. The arc structure reported by Sandholt *et al.* [2001, 2002] during a sharp northward rotation of the IMF was also seen in the conjugate DMSP data as accelerated electrons of 1–5 keV. Acceleration of plasma associated with reconnection has been reported by Woch and Lundin [1992] who found that for IMF northward (southward) the increase of the plasma bulk flow resulted in an ion energy increase of ~ 1 keV in the merging/current disruption region which corresponds to a location at the poleward (equatorward) edge of the cusp in the ionosphere. In principle the electrons would be accelerated too, but as this energy is gained by an increased bulk flow velocity this acceleration mechanism will not have any noticeable effect on the electron distribution. Basinska *et al.* [1992] observed electromagnetic spikes at the poleward edge of the cusp during northward IMF, but their electron measurements do not indicate any acceleration on the order of a few keV or energy fluxes in the 6–10 mW/m² range. Clauer *et al.* [1995] and Stauning *et al.* [1995] reported solar wind driven modulations of the ionospheric cusp current system that were accompanied by repeating pulses (~ 25 –30 min) of CNA enhancements in the same range (0.2–0.6 dB) as we observe, moving poleward. Their observations are mostly during southward IMF conditions and the poleward movement (0.5–1.0 km/s) of the current system and CNA (to ~ 77 – 78° invariant magnetic latitude) is attributed to changes in the IMF B_Y component. They interpret the field aligned currents to be caused by velocity shears associated with changing convection patterns and the pulses to be modulated by IMF B_Y variations.

[20] Although we find arcs involving higher electron energies than usually are reported from the cusp region we notice that discrete arcs and field aligned currents are not uncommon at the poleward edge of the cusp during northward IMF conditions. We also find it interesting that the discrete arcs found by Murphree *et al.* [1990] were strongly related to IMF $B_Y > 0$ and $B_X < 0$, which favors lobe reconnection at the front surface of the magnetotail in the Northern magnetosphere. Frey [2003] showed that high-latitude electron precipitation events tend to occur during IMF $B_Y > 0$ and $B_X < 0$ in the Northern hemisphere. The corresponding geometry in the Southern hemisphere would be $B_Y > 0$ and $B_X > 0$. In Figure 5 we have sketched the geometry of the field lines to show where the most anti-parallel field lines will appear. The magnetic tension force associated with the merged field lines will act on the plasma, creating the lobe convection cell and flow shears which will induce field-aligned currents [Sandholt *et al.*, 2001, 2002]. The high-latitude discrete arcs we observe are consistent with the current system one should expect during lobe reconnection. According to Iijima *et al.* [1984] an upward field aligned cusp current (i.e., in the cleft) will result from lobe reconnection (northward IMF) in the prenoon sector in the Southern hemisphere for IMF $B_Y > 0$. Both our events moved equatorward movement at ~ 0.5 km/s. We attribute this to erosion of field lines as the IMF turned southward. A similar transition from type 2 (lobe reconnection) to type 1 (dayside reconnection) aurora

caused by a rotation of the IMF was reported by Sandholt *et al.* [1998a].

5. Conclusion

[21] In this study we have reported two events of discrete dayside aurora at high latitudes controlled by solar wind changes. Our interpretation of the observations can be summarized as:

1. Discrete arcs formed at high latitudes ($\sim 77\text{--}79^\circ$). The onsets coincided with northward turnings of the IMF.

2. An average electron energy of 4–8 keV and energy deposition of 6–10 mW/m² were estimated from the combined optical and riometer data from ground and X-ray images from space. Although this region is usually associated with <1 keV electron precipitation, several studies have reported locally accelerated electrons of a few keV in this region.

3. We attribute the equatorward motion of the arcs at ~ 0.5 km/s to the IMF southward turning. Due to the uncertainties connected to the determination of the open-closed boundary we suggest two different scenarios involving different mechanisms that can explain our observations.

4. KH instabilities: The IMF northward turning moves the cusp location significantly poleward and the arcs are formed equatorward of the cusp due to KH instabilities at the inner edge of the LLBL. The subsequent equatorward movement is a response to the IMF southward turning which moves the boundaries back to lower latitudes.

5. Lobe reconnection: The geometry of the IMF and the Earth's magnetic field favored lobe reconnection on the front surface of the magnetotail in the Southern magnetosphere. These flux tubes have footprints poleward of the cusp. The precipitating electrons were probably accelerated by parallel electric fields resulting from converging horizontal electric fields associated with convection enhancements due to lobe reconnection. The subsequent equatorward motion is attributed to the IMF southward turning that favored reconnection at the dayside magnetosphere and erosion of magnetic field lines.

[22] **Acknowledgments.** This study was supported by the Norwegian Research Council (NFR). The work at the University of Maryland was supported by National Science Foundation grant OPP-9732662 and by Lockheed Martin subcontract SE70A0470. We acknowledge the World Data Center for Geomagnetism (T. Kamei), Kyoto, Japan for providing the preliminary Quick look *AE*, *AL* and *AU* indices. N. Østgaard wants to thank the staff of the NASA/GSFC Laboratory for Extraterrestrial Physics for their hospitality and support during his stay from June 2000 to September 2001 where most of this study was done.

[23] Arthur Richmond thanks David G. Sibeck and another reviewer for their assistance in evaluating this manuscript.

References

- Aksnes, A., J. Stadsnes, J. Bjordal, N. Østgaard, R. R. Vondrak, D. L. Detrick, T. J. Rosenberg, G. A. Germany, and D. Chenette, Instantaneous ionospheric global conductance maps during an isolated substorm, *Ann. Geophys.*, **20**, 1181–1191, 2002.
- Basinska, E. M., W. J. Burke, N. C. Maynard, W. J. Hughes, J. D. Winningham, and W. B. Hanson, Small-scale electrodynamic of the cusp with northward interplanetary magnetic field, *J. Geophys. Res.*, **97**, 6369–6379, 1992.
- Berkey, F. T., V. M. Driatskij, K. Henriksen, B. Hultqvist, D. Jelly, T. I. Shchuka, A. Theander, and J. Ylioniemi, A synoptic investigation of particle precipitation dynamics for 60 substorms in IQSY(1964–65) and IASY(1969), *Planet. Space Sci.*, **22**, 255–307, 1974.
- Clauer, C. R., P. Stauning, T. J. Rosenberg, E. Friis-Christensen, P. M. Miller, and R. J. Sitar, Observation of a solar-wind-driven modulation of the dayside ionospheric DPY current system, *J. Geophys. Res.*, **100**, 7697–7713, 1995.
- Clauer, C. R., A. J. Ridley, R. J. Sitar, H. J. Singer, A. S. Rodger, E. Friis-Christensen, and V. O. Papitashvili, Field line resonant pulsations associated with a strong dayside ionospheric shear convection flow reversal, *J. Geophys. Res.*, **102**, 4585–4596, 1997.
- Cowley, S. W. H., J. P. Morelli, and M. Lockwood, Dependence of convective flows and particle precipitation in the high-latitude dayside ionosphere and the X and Y components of the interplanetary magnetic field, *J. Geophys. Res.*, **96**, 5557–5564, 1991.
- Crooker, N. U., An evolution of anti-parallel merging, *Geophys. Res. Lett.*, **13**, 1063–1066, 1986.
- Denig, W. F., W. J. Burke, N. C. Maynard, F. J. Rich, B. Jacobsen, P. E. Sandholt, A. Egeland, S. Leontjev, and V. G. Vorobjev, Ionospheric signatures of dayside magnetopause transients: A case study using satellite and ground measurements, *J. Geophys. Res.*, **98**, 5969–5980, 1993.
- Detrick, D. L., and T. J. Rosenberg, A phased-array radiowave imager for studies of cosmic noise absorption, *Radio Sci.*, **25**, 325–338, 1990.
- Eather, R. H., and S. B. Mende, Airborne observations of auroral precipitation patterns, *J. Geophys. Res.*, **76**, 1746, 1971.
- Frey, H. U., Properties of localized high latitude dayside aurora, *J. Geophys. Res.*, **108**(A4), doi:10.1029/2002JA009332, in press, 2003.
- Iijima, T., T. A. Potemra, L. J. Zanetti, and P. F. Bythrow, Large-scale Birkeland currents in the dayside polar region during strongly northward IMF, *J. Geophys. Res.*, **89**, 7441, 1984.
- Lanzerotti, L. J., A. Shono, H. Fukunishi, and C. G. MacLennan, Long-period hydromagnetic waves at very high geomagnetic latitudes, *J. Geophys. Res.*, **104**, 28,423–28,435, 1999.
- Lepping, R. P., et al., The WIND magnetic field investigation, *Space Sci. Rev.*, **71**, 207–229, 1995.
- Mathews, D. L., T. J. Rosenberg, J. R. Benbrook, and E. A. Bering III, Dayside energetic electron precipitation over the south pole ($\gamma = 75^\circ$), *J. Geophys. Res.*, **93**, 12,941–12,945, 1988.
- Mende, S. B., H. U. Frey, J. H. Doolittle, L. Lanzerotti, and C. G. MacLennan, Dayside optical and magnetic correlation events, *J. Geophys. Res.*, **106**, 24,637–24,649, 2001.
- Murphree, J. S., R. D. Elphinstone, D. Hearn, and L. L. Cogger, Large scale high-latitude dayside auroral emissions, *J. Geophys. Res.*, **95**, 2345–2354, 1990.
- Newell, P. T., and C.-I. Meng, Mapping the dayside ionosphere to the magnetosphere according to particle precipitation characteristics, *Geophys. Res. Lett.*, **19**, 609–612, 1992.
- Ogilvie, K. W., et al., SWE, A comprehensive plasma instrument for the WIND spacecraft, *Space Sci. Rev.*, **71**, 55–77, 1995.
- Øieroset, M., H. Lühr, J. Moen, T. Moretto, and P. E. Sandholt, Dynamical auroral morphology in relation to ionospheric plasma convection and geomagnetic activity: Signatures of magnetopause X line dynamics and flux transfer events, *J. Geophys. Res.*, **101**, 13,275–13,292, 1996.
- Øieroset, M., P. E. Sandholt, W. F. Denig, and S. W. H. Cowley, Northward interplanetary magnetic field cusp aurora and high-latitude magnetopause reconnection, *J. Geophys. Res.*, **102**, 11,349–11,362, 1997.
- Østgaard, N., J. Bjordal, J. Stadsnes, and E. Thorsen, PIXIE data processing at the University of Bergen, *Tech. Rep. 1999-05*, Univ. of Bergen, Bergen, Norway, 1999a.
- Østgaard, N., J. Stadsnes, J. Bjordal, R. R. Vondrak, S. A. Cummer, D. Chenette, G. K. Parks, M. J. Brittacher, and D. L. McKenzie, Global scale electron precipitation features seen in UV and X rays during substorms, *J. Geophys. Res.*, **104**, 10,191–10,204, 1999b.
- Østgaard, N., J. Stadsnes, J. Bjordal, R. R. Vondrak, S. A. Cummer, D. Chenette, M. Schulz, and J. Pronko, Cause of the localized maximum of X-ray emission in the morning sector: A comparison with electron measurements, *J. Geophys. Res.*, **105**, 20,869, 2000.
- Østgaard, N., J. Stadsnes, J. Bjordal, G. A. Germany, G. K. Parks, R. R. Vondrak, S. A. Cummer, D. Chenette, and J. Pronko, Auroral electron distributions derived from combined UV and X-ray emissions, *J. Geophys. Res.*, **106**, 26,081–26,090, 2001.
- Rairden, R. L., and S. B. Mende, Properties of 6300 Å auroral emissions at south pole, *J. Geophys. Res.*, **94**, 1402, 1989.
- Rees, M. H., Auroral ionization and excitation by incident energetic electrons, *Planet. Space Sci.*, **11**, 1209–1218, 1963.
- Rees, M. H., *Physics and Chemistry of the Upper Atmosphere*, Cambridge Univ. Press, Cambridge, U. K., 1989.
- Rees, M. H., and D. Luckey, Auroral electron energy derived from ratio of spectroscopic emissions, 1, Model computations, *J. Geophys. Res.*, **79**, 5182, 1974.

- Rees, M. H., and R. G. Roble, Excitation of $O(^1D)$ atoms in aurorae and emissions of the [OI] 6300 Å line, *Can. J. Phys.*, 1608–1613, 1986.
- Roble, R. G., and M. H. Rees, Time-dependent studies of the aurora: Effects of particle precipitation on the dynamic morphology of ionospheric and atmospheric properties, *Planet. Space Sci.*, 25, 991–1010, 1977.
- Sandholt, P. E., and P. T. Newell, Ground and satellite observations of an auroral event at the cusp/cleft equatorward boundary, *J. Geophys. Res.*, 97, 8685–8691, 1996.
- Sandholt, P. E., C. J. Farrugia, M. Øieroset, P. Stauning, and S. W. H. Cowley, Auroral signature of lobe reconnection, *Geophys. Res. Lett.*, 23, 1725–1728, 1996.
- Sandholt, P. E., C. J. Farrugia, J. Moen, and S. W. H. Cowley, Dayside auroral configuration: Responses to southward and northward rotations of the interplanetary magnetic field, *J. Geophys. Res.*, 103, 20,279–20,295, 1998a.
- Sandholt, P. E., C. J. Farrugia, J. Moen, O. Norberg, B. Lybekk, T. Sten, and T. Hansen, A classification of dayside auroral forms and activities as a function of interplanetary magnetic field orientation, *J. Geophys. Res.*, 103, 23,325–23,345, 1998b.
- Sandholt, P. E., C. J. Farrugia, S. W. H. Cowley, M. Lester, and J. C. Cerisier, Excitation of transient lobe cell convection and auroral arcs at the cusp poleward boundary during a transition of the interplanetary magnetic field from south to north, *Ann. Geophys.*, 19, 487, 2001.
- Sandholt, P. E., C. J. Farrugia, J. Moen, and W. F. Denig, The cusp in rapid transition, *J. Geophys. Res.*, 107(A12), 1427, doi:10.1029/2001JA009214, 2002.
- Sandholt, P. E., et al., Dynamic cusp aurora and associated pulsed reverse convection during northward interplanetary magnetic field, *J. Geophys. Res.*, 105, 12,869–12,894, 2000.
- Shue, J. H., J. K. Chao, H. C. Fu, C. T. Russell, P. Song, K. K. Khurana, and H. J. Singer, A new functional form to study the solar wind control of the magnetopause size and shape, *J. Geophys. Res.*, 102, 9497–9511, 1997.
- Shue, J.-H., et al., Magnetopause location under extreme solar wind conditions, *J. Geophys. Res.*, 103, 17,691–17,700, 1998.
- Sibeck, D. G., et al., Comprehensive study of the magnetospheric response to a hot flow anomaly, *J. Geophys. Res.*, 104, 4577–4593, 1999.
- Sitar, R. J., J. B. Baker, C. R. Clauer, A. J. Ridley, J. A. Cumnoock, V. O. Paptashvili, J. Spann, M. J. Brittner, and G. K. Parks, Multi-instrument analysis of the ionospheric signatures of a hot flow anomaly occurring on July 24, 1996, *Geophys. Res. Lett.*, 103, 23,357–23,372, 1998.
- Stauning, P., C. R. Clauer, T. J. Rosenberg, E. Friis-Christensen, and R. Sitar, Observations of solar-wind driven progression of interplanetary magnetic field B_y -related dayside ionospheric disturbances, *J. Geophys. Res.*, 100, 7567–7585, 1995.
- Thomsen, M. F., J. T. Gosling, S. A. Fuselier, S. J. Bame, and C. T. Russell, Hot diamagnetic cavities upstream from the Earth's bow shock, *J. Geophys. Res.*, 91, 2961–2973, 1986.
- Tsyganenko, N. A., Modelling the Earth's magnetospheric magnetic field confined within a realistic magnetopause, *J. Geophys. Res.*, 100, 5599–5612, 1995.
- Vondrak, R. R., and M. J. Baron, Radar measurements of latitudinal variation of auroral ionization, *Radio Sci.*, 11, 939, 1976.
- Vondrak, R. R., and R. Robinson, Inference of high-latitude ionization and conductivity from AE-C measurements of auroral electron fluxes, *J. Geophys. Res.*, 90, 7505–7512, 1985.
- Weatherwax, A. T., H. B. Vo, T. J. Rosenberg, S. B. Mende, H. U. Frey, L. J. Lanzerotti, and C. G. MacLennan, A dayside ionospheric absorption perturbation in response to a large deformation of the magnetopause, *Geophys. Res. Lett.*, 26, 517–520, 1999.
- Woch, J., and R. Lundin, Magnetosheath plasma precipitation in the polar cap and its control by the interplanetary magnetic field, *J. Geophys. Res.*, 97, 1421–1430, 1992.
-
- D. L. Detrick, Institute for Physical Science and Technology University of Maryland, College Park, MD 20742-2431, USA.
- H. U. Frey, Space Sciences Laboratory, University of California, Berkeley, California, CA 94720-7450, USA.
- S. E. Håland, ISSI, Hallerstrasse 6, CH 3012, Bern, Switzerland.
- J. Stadsnes, University of Bergen, Allegt 55, N-5007, Bergen, Norway.
- S. B. Mende, Space Sciences Laboratory, University of California, Berkeley, California, CA 94720-7450, USA.
- N. Østgaard, Space Sciences Laboratory, University of California, Berkeley, California, CA 94720-7450, USA. (nikost@ssl.berkeley.edu)
- T. J. Rosenberg, Institute for Physical Science and Technology University of Maryland, College Park, MD 20742-2431, USA.
- R. R. Vondrak, Laboratory for Extraterrestrial Physics, Code 690, Building 2, NASA/GSFC, Greenbelt, MD 20771, USA.

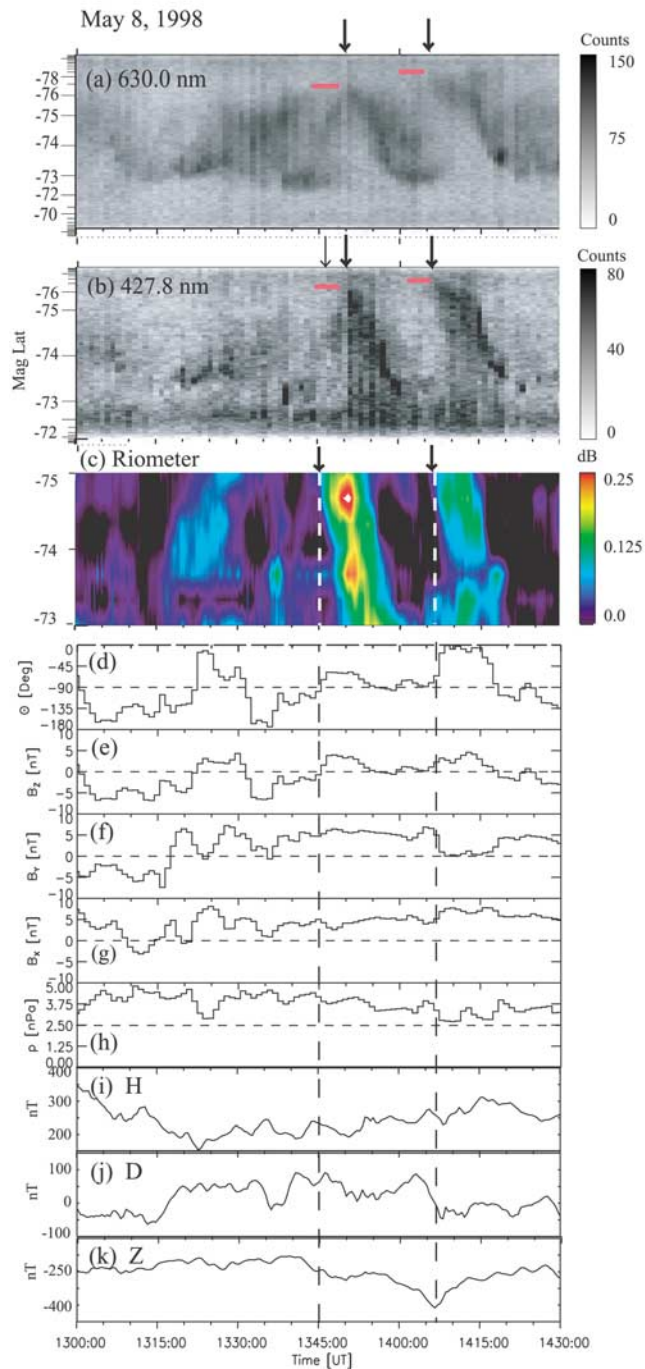


Figure 2. The three upper panels show meridian slices of the ASC and riometer data from the South Pole station, presented as keograms. (a) 630.0 nm emissions (<1 keV electrons). (b) 427.8 nm emissions (~ 10 keV electrons). (c) 38.2 MHz CNA (~ 10 – 100 keV electrons). Arrows indicate the onset times of the high latitude precipitation. Red (black) horizontal lines indicate the latitude of the onsets. The five next panels show the solar wind data. (d) θ is the IMF clock angle from 0° (northward) to 180° (southward). (e) IMF B_z (f) IMF B_y (g) IMF B_x (h) Solar wind dynamic pressure. Dashed line indicates average solar wind pressure. The three bottom panels (i–k) show the magnetic data from the South Pole station.

May 8, 1998

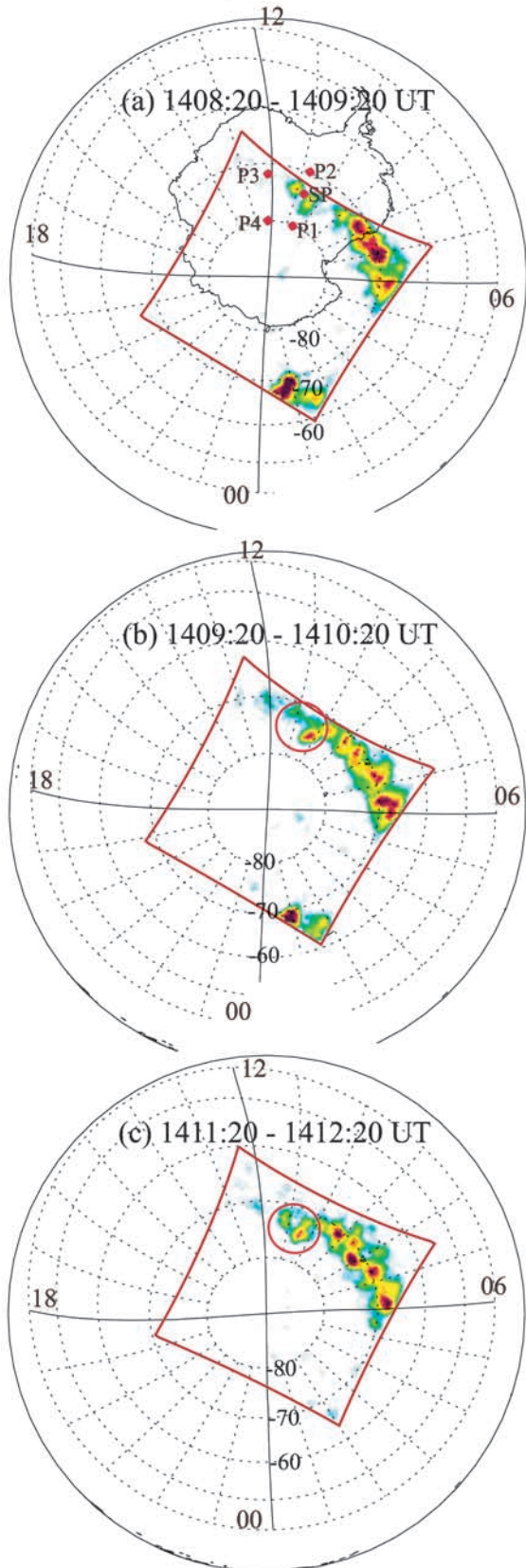


Figure 3. (opposite) 2.5–9.0 keV X-ray images on a CGM grid, 1 min time resolution from (a) 1408:20–1409:20 UT (b) 1409:20–1410:20 UT and (c) 1411:20–1412:20. The distorted red squared box indicates PIXIE FOV and the large red circle in (b) and (c) indicates the ASC FOV. The South Pole station and the AGO stations are indicated in (a).